*SF2A 2012*
*S. Boissier, P. de Laverny, N. Nardetto, R. Samadi, D. Valls-Gabaud and H. Wozniak (eds)*

# NON-LTE EFFECTS ON THE IONIZATION EQUILIBRIUM OF FE I/FE II: APPLICATION TO THE RED GIANTS OF CARINA DSPH GALAXY

T. Merle[1], M. Fabrizio[2], F. Thévenin[1], M. Nonino[3], G. Bono[2,4] and Carina Project Team

**Abstract.** In the context of the Carina Project, we re-analyze the iron abundances of 44 red giants of the Carina dSph galaxy to derive its metallicity distribution function. The abundance analyses were performed with the LTE spectrum synthesis fitting method using ESO/VLT high resolution spectra. Using Fe I lines, we obtained stellar metallicities of $\sim$ 0.1 dex lower than using Fe II lines. This discrepancy is classically interpreted as an error on the surface gravity (based on photometry and evolutionary tracks) which is removed by changing gravity until Fe I abundances match Fe II ones. However, the NLTE mechanism of over-ionization regarding LTE can also explain this discrepancy in giant stars. To support this idea, we performed NLTE computations with a Fe I/II model atom and show that this discrepancy is well reproduced. NLTE computations also highlight large discrepancies in individual lines of Fe I and Fe II.

Keywords: abundances, metallicity, Carina galaxy, dSph galaxies, NLTE analysis

## 1 Observations and data reduction

The high-resolution spectra for Carina red giants adopted in this investigation were retrieved from the ESO Scientific Archive ($R \sim 38000$ and $15 \leq S/N \leq 45$). We selected spectra from four different ESO/VLT observing programs collected with either UVES (slit mode, 9) or FLAMES/GIRAFFE-UVES (multifiber mode, 80). We ended up with a sample of 72 stars, located in the central region of Carina dSph galaxy and covering the bright portion of the red giant branch (see Fig. 1 on left). The UVES spectra (red arm, centered at 5800 Å) were reduce using IRAF. For a more detailed explanation on the observations, data reduction, and radial velocity determination see Fabrizio et al. (2011, 2012).

## 2 LTE spectroscopic analysis

The iron abundance analysis was performed following the classical spectrum-synthesis method for both Fe I and Fe II lines, but with one difference: we did not impose LTE ionization equilibrium between the Fe I and the Fe II lines (e.g. Kraft & Ivans 2003). We used the effective temperature $T_{\rm eff}$ and surface gravity $\log g$ (see Fig. 1 on right) determined from the optical photometry (Bono et al. 2010; Stetson et al. 2011) and BaSTI isochrones (Pietrinferni et al. 2004, 2006). Typical uncertainties are 70 K and 0.2 dex. The synthetic spectra were computed using the 1D, plane-parallel, LTE, radiative transfer code MOOG (2009 version, Sneden 1973) with VALD line list (Kupka et al. 2000) and MARCS model atmospheres (Gustafsson et al. 2008). We used a constant microturbulent velocity of 2 km s$^{-1}$ (mean value from Shetrone et al. 2003). The resulting accuracy of the line fits ranges from 0.10 to 0.15 dex.

## 3 Metallicity Distribution Function corrected for NLTE effects

We obtained the iron abundances for $N_\star = 44$ red giants using Fe I lines and for $N_\star = 27$ using Fe II lines. The metallicity distribution function (MDF) is shown on left panel of Fig. 2; with a weighted mean metallicity of

[1] Laboratoire Lagrange, UMR7293, Université de Nice Sophia-Antipolis, CNRS, Observatoire de la Côte d'Azur, 06300 Nice, France
[2] Dipartimento di Fisica, Università di Roma Tor Vergata, via della Ricerca Scientifica 1, 00133 Rome, Italy
[3] INAF - Osservatorio Astronomico di Trieste, via G.B. Tiepolo 11, 40131 Trieste, Italy
[4] INAF - Osservatorio Astronomico di Roma, via Frascati 33, Monte Porzio Catone, Rome, Italy

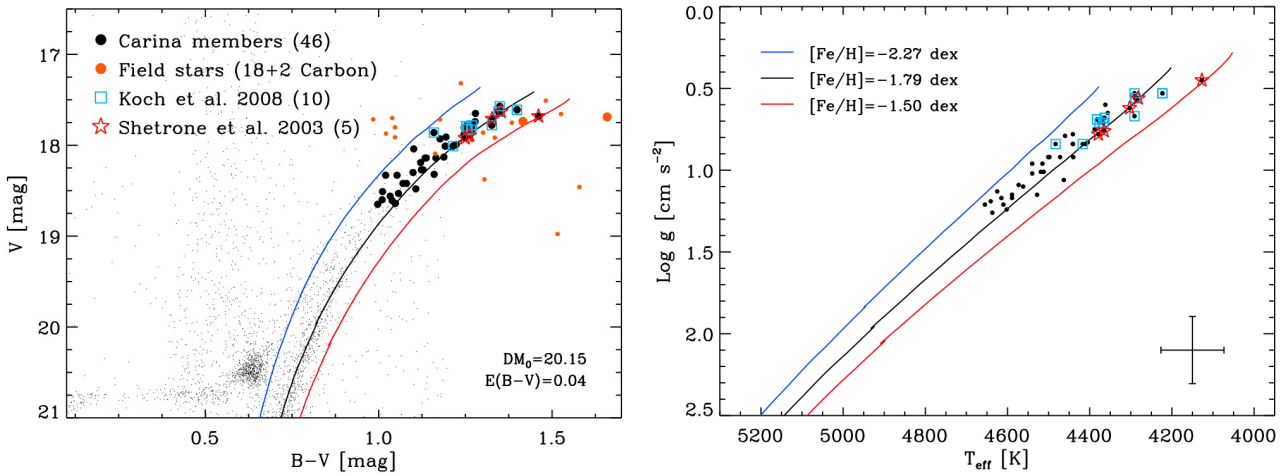


**Fig. 1. Left:** $V$, $B-V$ color-magnitude diagram of the spectroscopic targets. The black dots are the UVES targets with a radial velocity between 180 and 260 km s$^{-1}$ (Carina candidate members), orange dots are targets with outside radial velocities. The radial velocities were measured using a dozen of heavy-element lines ranging from 6136 to 6200 Å. Two large orange dots are two carbon stars. Isochrones from BaSTI (Pietrinferni et al. 2004, 2006) at 12 Gyr are displayed for [Fe/H] = −1.50, −1.79 and −2.27 in red, black and blue, respectively. **Right:** same as the left, but the targets are in the effective temperature vs surface gravity plane.

| | Fe I | | | Fe II | | |
|---|---|---|---|---|---|---|
| $N_\star$ | $\mu_{\rm [Fe\,I/H]}$ | $\mu^{\rm weighted}_{\rm [Fe\,I/H]}$ | $\sigma_{\rm [Fe\,I/H]}$ | $\mu_{\rm [Fe\,II/H]}$ | $\mu^{\rm weighted}_{\rm [Fe\,II/H]}$ | $\sigma_{\rm [Fe\,II/H]}$ |
| 27 | $-1.85 \pm 0.15$ | $-1.84 \pm 0.02$ | 0.23 | $-1.76 \pm 0.23$ | $-1.72 \pm 0.04$ | 0.24 |
| 44 | $-1.93 \pm 0.17$ | $-1.90 \pm 0.02$ | 0.30 | $-1.84 \pm 0.21$ | $-1.80 \pm 0.02$ | 0.29 |

**Table 1.** Parameters of the MDFs as a function of number of stars and the adopted iron lines.

−1.90 and a spread of 0.30 dex. The weighted mean metallicity is computed using individual uncertainties on each star. The iron abundances deduce from Fe I lines are systematically lower than those obtained from Fe II lines (Table 3, first line). This difference is explained by assuming that Fe II is not affected by NLTE effects, at least on the ionization equilibrium, since Fe II is the dominant ionization stage in red giants. To account for NLTE effects on Fe I abundance determination, we estimated [Fe II/H] as a linear function of [Fe I/H] and corrected [Fe I/H] abundances (Table 3, second line). Then we estimated the MDF free from NLTE effects on Fe I (right panel of Fig. 2).

## 4 Comparison with Non-LTE models

To support the assumption that the difference in abundance is due to NLTE effect, we compute LTE ($W^*$) and NLTE ($W$) equivalent widths with MULTI (Carlsson 1986, version 2.2), for two typical model atmospheres of Carina red giants, using a model atom of Fe I/II (Collet et al. 2005). We neglected inelastic collisions with hydrogen assuming that they are less efficient than in dwarf stars. The atomic data are from: NIST for the energy levels, Nave et al. (1994); Kurucz & Bell (1995); Thévenin (1989) for oscillator strengths, Bautista (1997) for photo-ionisation cross sections, and van Regemorter (1962) for inelastic collisions with free electrons.

For iron lines between 4000 and 9000 Å, we selected weak lines ($W < 100$ mÅ) of Fe I and Fe II, and used the relation given NLTE abundance correction as a function of the ratio $W/W^*$ (from the curve of growth theory, see e.g. Merle et al. (2011) for more details):

$$\Delta[\mathrm{Fe/H}] = [\mathrm{Fe/H}] - [\mathrm{Fe/H}]^* \approx -\log(W/W^*). \quad (4.1)$$

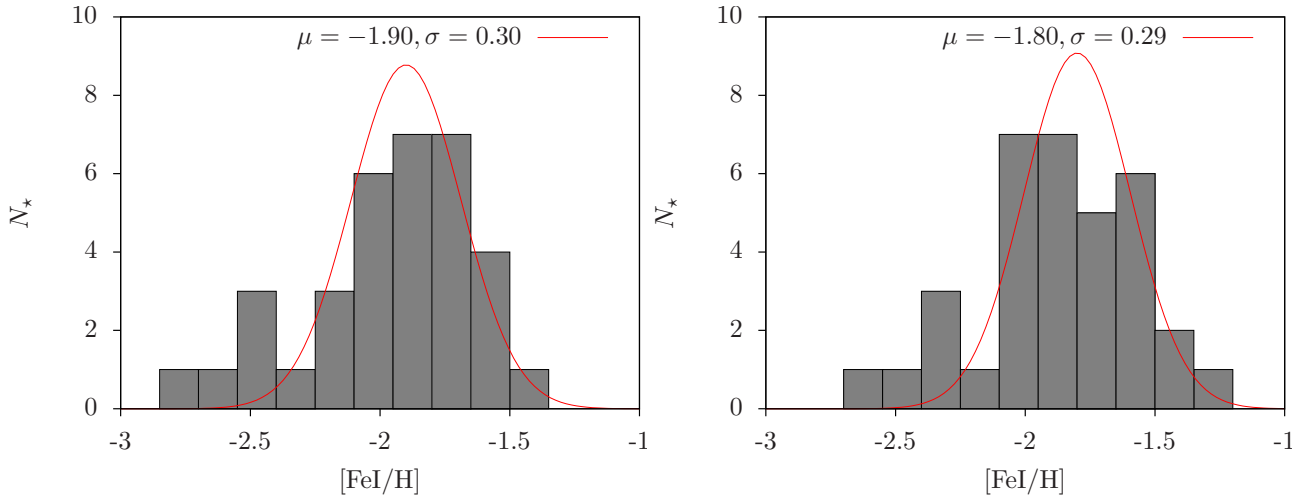


**Fig. 2.** MDFs of dSph Carina stars. **Left:** before NLTE correction. **Right:** after NLTE correction (using Fe II lines).

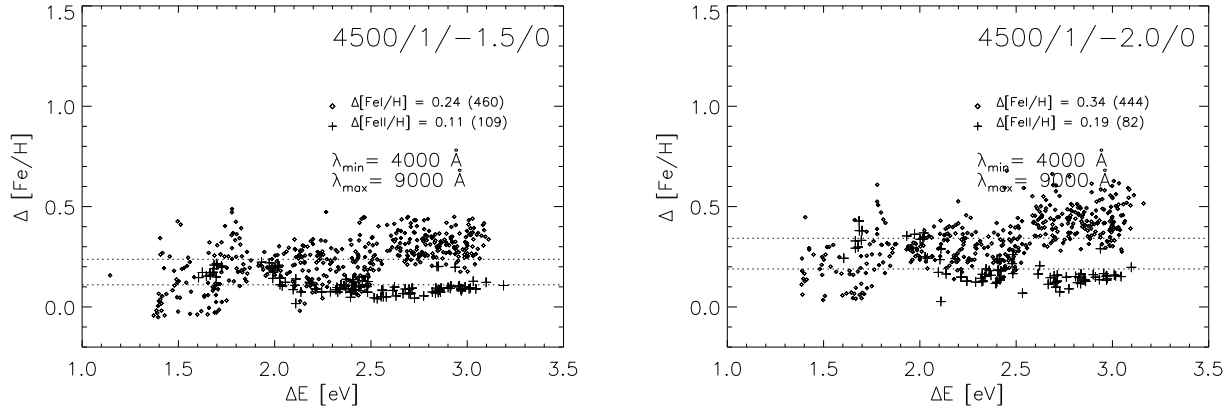


**Fig. 3.** Theoretical NLTE corrections Δ[Fe/H] for Fe I (diamonds) and Fe II (crosses) as a function of transition energy $\Delta E$ for two typical model atmospheres of Carina giant stars with $T_{\rm eff} = 4500$ K, $\log g = 1.0$, and [Fe/H] $= -1.50$ (**left**) or [Fe/H] $= -2.00$ (**right**). The means are given for the number of transitions written in parenthesis and plotted as dotted lines. The transitions considered have wavelengths between 4000 and 9000 Å.

The theoretical Non-LTE abundance corrections Δ[Fe/H] for the two ionization stages of iron are shown in Fig. 3 for two red giant model atmospheres: $T_{\rm eff} = 4500$ K, $\log g = 1.0$, [Fe/H] $= -1.50$ (left) and [Fe/H] $= -2.0$ (right). For Fe I lines, we noticed an increase of NLTE effects with the transition energy which is due to fact that the radiation dominate over the collisions at high transition energy. The Fe II lines are less affected by NLTE effects as expected since Fe II is the dominant ionization stage at these temperature and pressure (House 1964). Moreover, the NLTE effects are more important for the metal-poor model both for Fe I and Fe II. We found significant mean relative difference between [Fe I/H] and [Fe II/H] NLTE theoretical abundances of the order of 0.1 dex. The ensuing linear regression is in good agreement with the linear regression based on the observations analyzed in LTE (Fig. 4) without forcing ionization equilibrium between Fe I and Fe II to follow Saha's law. Furthermore, NLTE abundance corrections are also found on the excitation equilibria and they represent an upper limit for NLTE effects on iron, since inelastic collisions with hydrogen were neglected.

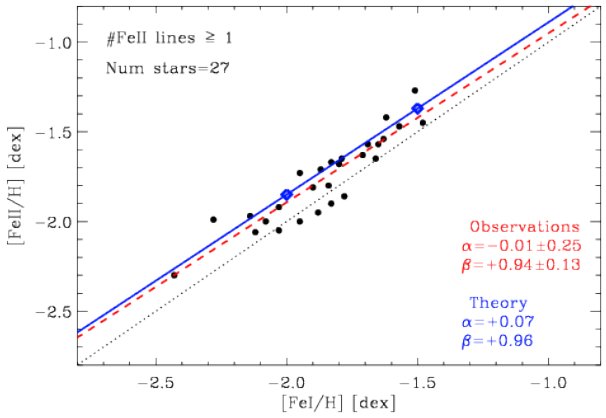


**Fig. 4.** NLTE effects on ionization equilibrium. [Fe II/H] as a function of [Fe I/H]. Comparison between abundances deduce from LTE analysis (black dots) and NLTE models (blue diamonds). Linear regression $[\mathrm{Fe\,II/H}] = \alpha + \beta[\mathrm{Fe\,I/H}]$ is given for observations (dashed red line) and theory (solid blue line).

## 5 Conclusion

We determined the metallicity distribution function for a sample of 44 Carina RG stars. Our sample is more than a factor of four larger than any previous spectroscopic investigation based on high-resolution spectra. Detailed comparisons (Fabrizio et al. 2012) for stars in common with previous investigations (Shetrone et al. 2003; Koch et al. 2008, 2006; Lemasle et al. 2012; Venn et al. 2012) show that our iron abundance determinations are lower even when using Fe II lines only. We corrected for NLTE effects on the ionization equilibrium and we found a weighted mean metallicity of [Fe/H] = 1.80 and a dispersion of $\sigma = 0.29$ dex.

However, the current data do not allow us to determine whether the spread is either atmospheric, i.e., caused by a difference in the mean metallicity between the old and the intermediate-age population, or by measurement errors. To assess whether the different stellar populations are also characterized by different mean metallicities, new spectra with high S/N down to the red clump (intermediate-mass) and to the red horizontal branch (low-mass) stars are required.

## References

Bautista, M. A. 1997, A&AS, 122, 167
Bono, G., Stetson, P. B., Walker, A. R., et al. 2010, PASP, 122, 651
Carlsson, M. 1986, Uppsala Astronomical Observatory Reports, 33
Collet, R., Asplund, M., & Thévenin, F. 2005, A&A, 442, 643
Fabrizio, M., Merle, T., Thévenin, F., et al. 2012, PASP, 124, 519
Fabrizio, M., Nonino, M., Bono, G., et al. 2011, PASP, 123, 384
Gustafsson, B., Edvardsson, B., Eriksson, K., et al. 2008, A&A, 486, 951
House, L. L. 1964, ApJS, 8, 307
Koch, A., Grebel, E. K., Gilmore, G. F., et al. 2008, AJ, 135, 1580
Koch, A., Grebel, E. K., Wyse, R. F. G., et al. 2006, AJ, 131, 895
Kraft, R. P. & Ivans, I. I. 2003, PASP, 115, 143
Kupka, F. G., Ryabchikova, T. A., Piskunov, N. E., Stempels, H. C., & Weiss, W. W. 2000, Baltic Astronomy, 9, 590
Kurucz, R. L. & Bell, B. 1995, Atomic line list CD-ROM (Cambridge, MA: Smithsonian Astrophysical Observatory)
Lemasle, B., Hill, V., Tolstoy, E., et al. 2012, A&A, 538, A100
Merle, T., Thévenin, F., Pichon, B., & Bigot, L. 2011, MNRAS, 418, 863
Nave, G., Johansson, S., Learner, R. C. M., Thorne, A. P., & Brault, J. W. 1994, ApJS, 94, 221

Pietrinferni, A., Cassisi, S., Salaris, M., & Castelli, F. 2004, ApJ, 612, 168
Pietrinferni, A., Cassisi, S., Salaris, M., & Castelli, F. 2006, ApJ, 642, 797
Shetrone, M., Venn, K. A., Tolstoy, E., et al. 2003, AJ, 125, 684
Sneden, C. 1973, ApJ, 184, 839
Stetson, P. B., Monelli, M., Fabrizio, M., et al. 2011, The Messenger, 144, 32
Thévenin, F. 1989, A&AS, 77, 137
van Regemorter, H. 1962, ApJ, 136, 906
Venn, K. A., Shetrone, M. D., Irwin, M. J., et al. 2012, ApJ, 751, 102